Original article / Оригинальная статья
УДК 551.242
DOI: http://dx.doi.org/10.21285/2686-9993-2021-44-1-8-29

Mixed crystalline basement of Junggar basin revealed by wide-angle seismic evidence*

© Junmeng Zhao[a], Wenjiao Xiao[b], Xinfa Chen[c], Xiaojun Wang[d], Yong Song[e], Baoli Bian[f], Xiankang Zhang[g], Irina P. Strelchenko[h], Qiang Xu[i], Heng Zhang[j], Yingcai Zheng[k], Hongbing Liu[l], Bhupati Neupane[m], Zongjin Ma[n]

[a,i,j,l]*Center for Excellence in Tibetan Plateau Earth Sciences, Chinese Academy of Sciences, Beijing, China*
[a,h,i,j,l,m]*Institute of Tibetan Plateau Research, Chinese Academy of Sciences, Beijing, China*
[a,b,h,m]*University of Chinese Academy of Sciences, Beijing, China*
[b]*Institute of Geology and Geophysics, Chinese Academy of Sciences, Beijing, China*
[c,d,e,f]*Xinjiang Oilfield Company, Karamay, China*
[g]*Center for Geophysical Exploration, China Earthquake Administration, Zhengzhou, China*
[k]*Massachusetts Institute of Technology, Cambridge, United States of America*
[n]*Institute of Geology, China Earthquake Administration, Beijing, China*
[h]*Irkutsk National Research Technical University, Irkutsk, Russia*

Abstract: A wide-angle seismic reflection / refraction survey along a ~ 600 km long transect through the Junggar basin from Emin to Qitai allows to receive several images near N-S trending blind faults, which are located at the lower part of the upper crust, the middle crust and the lower crust within the basin and cut up the Moho. These faults, with high seismic velocity and without obvious dislocation, are considered as "extensional faults" formed by north-south compression and east-west extension. These deeply rooted faults provide channels via which basic to ultra-basic materials from upper mantle migrate into the crust and mix up with the crustal material causing thin thickness, high seismic velocity, high density and high magnetic intensity after cooling in the crust of the basin.

Keywords: Junggar Basin, seismic wide-angle reflection / refraction profiling, velocity structure, density structure, magnetic intensity structure, geological interpretation

Acknowledgements: This research was jointly supported by "Major National Science and Technology Projects for the Development of Large Oil and Gas Fields and Coalbed Methane (2011ZX05003-005)", "National Science Foundation of China (41888101)", "Strategic Priority Research Program (A) of the Chinese Academy of Sciences (Grant No. XDA20070302)", "Joint Research Projects between Pakistan Science Foundation and National Natural Science Foundation of China (Grant No. 41661144026)", and "Exploration and Research on Continental Subduction in Western Himalayan Syntaxis (Grant No. 41490611)". We are grateful to researchers in the Center for Geophysical Exploration CEA for their hard work in acquiring the wide-angle reflection/refraction data. We also thank Dr. Zhang Guoqing for the gravitational and geomagnetic data.

For citation: Zhao Junmeng, Xiao Wenjiao, Chen Xinfa, Wang Xiaojun, Song Yong, Bian Baoli, et al. Mixed crystalline basement of Junggar basin revealed by wide-angle seismic evidence. *Nauki o Zemle i nedropol'zovanie = Earth sciences and subsoil use.* 2021;44(1):8–29. (In Russ.) https://doi.org/10.21285/2686-9993-2021-44-1-8-29

*The article was provided by the Earth Science Frontiers journal within the framework of the agreement between the editorial boards of Irkutsk National Research Technical University (Irkutsk, Russia) and China University of Geosciences (Beijing, China) on the exchange of open access scientific papers.

Смешанный кристаллический фундамент Джунгарской котловины, выявленный методом широкоугольной сейсморазведки*

© Цзюньмэн Чжао[a], Вэньцзяо Сяо[b], Синьфа Чэнь[c], Сяоцзюнь Ван[d], Юн Сун[e], Баоли Бянь[f], Сянькан Чжан[g], И.П. Стрельченко[h], Цян Сюй[i], Хэн Чжан[j], Инцай Чжэн[k], Хунбин Лю[l], Бхупати Неупане[m], Чжунцзинь Ма[n]

[a,i,j,l]Центр передового опыта наук о Земле Тибетского плато, Китайская академия наук, г. Пекин, Китай
[a,h,i,j,l,m]Институт изучения Тибетского плато, Китайская академия наук, г. Пекин, Китай
[a,b,h,m]Университет Китайской академии наук, г. Пекин, Китай
[b]Институт геологии и геофизики, Китайская академия наук, г. Пекин, Китай
[c,d,e,f]Синьцзянская нефтяная компания, г. Карамай, Китай
[g]Центр геофизических исследований Сейсмологического управления Китая, г. Чжэнчжоу, Китай
[k]Массачусетский технологический институт, г. Кембридж, Соединенные Штаты Америки
[n]Институт геологии Сейсмологического управления Китая, г. Пекин, Китай
[h]Иркутский национальный исследовательский технический университет, г. Иркутск, Россия

Резюме: Широкоугольная сейсморазведка методом отраженных / преломленных волн вдоль линии поперечного разреза протяженностью ~ 600 км через Джунгарский бассейн от Эминя до Цитая позволяет получить изображение нескольких слепых разломов с простиранием с севера на юг, которые расположены в нижней части верхней коры, в средней и нижней частях коры в пределах бассейна и разрезают Мохо. Эти разломы, обладающие высокой сейсмической скоростью и не имеющие явной дислокации пластов, считаются «разломами растяжения», образованными сжатием с севера на юг и растяжением с востока на запад. Эти глубоко залегающие разломы обеспечивают каналы для основных и ультраосновных материалов из верхней мантии, которые мигрируют в кору и смешиваются с материалом коры, в результате чего кора бассейна становится тонкой и приобретает высокую сейсмическую скорость, высокую плотность и высокую магнитную интенсивность после охлаждения.

Ключевые слова: Джунгарский бассейн, широкоугольное профилирование методом отраженных / преломленных волн, структура скорости, структура плотности, структура магнитной напряженности, геологическая интерпретация

Благодарности: Это исследование выполнено при совместной поддержке программы «Крупные национальные научно-технические проекты по разработке крупных месторождений нефти и газа, а также метана угольных пластов (2011ZX05003-005)», Национального научного фонда Китая (41888101), грантов «Программа стратегических приоритетных исследований (A) Китайской академии наук (грант № XDA20070302)», «Совместные исследовательские проекты Пакистанского научного фонда и Национального фонда естественных наук Китая (грант № 41661144026)» и «Разведка и исследование континентальной субдукции в Западных Гималаях (грант № 41490611)». Мы благодарим исследователей Центра геофизических исследований CEA за их усердную работу по получению данных широкоугольного отражения / преломления. Мы также благодарим доктора Гоцин Чжан за предоставление гравитационных и геомагнитных данных.

Для цитирования: Чжао Цзюньмэн, Сяо Вэньцзяо, Чэнь Синьфа, Ван Сяоцзюнь, Сун Юн, Бянь Баоли [и др.]. Смешанный кристаллический фундамент Джунгарской котловины, выявленный методом широкоугольной сейсморазведки. *Науки о Земле и недропользование.* 2021. Т. 44. № 1. С. 8–29. https://doi.org/10.21285/2686-9993-2021-44-1-8-29

Introduction

The Junggar Basin is a large-scale intracontinental superimposed basin in northern Xinjiang since Permian [1–3]. It is the most promising area for petroleum prospects in China. In the past decades, the researches on the Junggar basin have given profound results dealing with the tectonic background and the evidence for existing theories [4–7]. Although a lot of geophysical and geological studies have been carried out since the 1980s, there are still many divergences of view in basin's tectonic evolution and the basement structure.

Xiao et al. [8] divided the evolution of the Junggar basin into several stages: the early Paleozoic intra-oceanic arc evolution, the Early

* Статья была предоставлена редакцией журнала Earth Science Frontiers в рамках соглашения между редакциями Иркутского национального исследовательского технического университета (г. Иркутск, Россия) и Китайского геологического университета (г. Пекин, Китай) об обмене научными статьями открытого доступа.

Devonian and later Middle Devonian rifting evolution of the Junggar ocean, formed from the rifting of the early Paleozoic folded basement, the relic ocean from Later Devonian to late Carboniferous, and the final accretion orogeny in the late Carboniferous-early Permian. Wu [9] considered that it was a rift in Permian, a depression in Triassic-Old Tertiary, and a contraction and uplift stage after Neogene. You [10] divided the basin into rift stage in Carboniferous-Triassic, central uplift stage in Jurassic and piedmont depression stage after Cretaceous. Zhao [11] divided the basin into fault depression stage in Permian and Triassic, depression stage in Jurassic-Old Tertiary and shrinkage-uplift stage after Neogene. Xiao et al. [12] considered that the Late Carboniferous-Early Permian was a marine foreland basin. Yang et al. [13] also classified the Early Permian as marine foreland, the Late Permian and Neogene-Quaternary as continental foreland, and the Triassic-Paleogene as oscillating continental basin. The main differences in the above-mentioned division opinions lie in the understanding of whether the nature of the basin is tensional or compressive in the Early Permian and the nature of the depression basin in the Late Permian-Old Tertiary. These differences have not narrowed, but have widened in recent years. Sun [14] advocates that we should abandon the understanding that the early basin is collapse or tension and consider Junggar as a Carboniferous-Permian foreland basin based on the Triassic-Jurassic intracontinental further subsidence, since the Cretaceous is mainly the typical pre-revival period continental basin, which unified only in the late Cenozoic. On the contrary, Chen et al. considered that Junggar Basin was a rift basin in the early stage (P), a craton basin in the middle stage (T-E), and a compression basin in the late stage (N-Q).

The basin's basement composition is also a controversial topic in the international community. Some researchers proposed that the central part of the Junggar basin is composed of a conjectural craton nucleus [1, 15]. Some others interpreted the basin as a trapped oceanic lithosphere [4], a relict back-arc basin [16] or deformed Altai Paleozoic rocks [17].

According to previous geophysical research in northwestern China, the average crustal thickness of the Junggar basin is about 50 km, while those of the Tarim basin and the Qaidam basin are ~ 55 km [18, 19] and ~ 60 km [20], respectively. The average P-wave velocity is 6.3 km/s in the Junggar basin [21], about 6.0 km/s in the Tarim basin [19], and about 5.8 km/s in the Qaidam basin [20]. Therefore, the Junggar basin has a thinner crustal thickness and a higher average crustal velocity than the Tarim and Qaidam basins. The formation mechanism for such characteristics, as well as the high geomagnetic anomalies distributed in the central part of the basin, is not well understood.

Recently, a comprehensive geophysical survey along a ~ 600 km long transect through the Junggar basin from Emin to Qitai was carried out (Fig. 1). Along the profile, a wide-angle seismic reflection/refraction was carried out to obtain 2D velocity structure of the crust and upper most mantle. Based on the 2D velocity structure as evidence for designing the starting model of the 2D density structure and 2D magnetic intensity structure and constrained by gravitational and geomagnetic anomalies along the profile, the density and magnetic intensity structure were obtained. Finally, we proposed a comprehensive geological interpretation.

Seismic data and processing

Recently, a seismic reflection/refraction profile as part of the ANTILOPE project was carried out to constrain the seismic velocity structure and physical properties of the crust and upper most mantle (Fig. 1). The profile crosses the Junggar basin from Emin in the northwest to Qitai in the southeast margins of the basin. The geometry of the profile was designed to optimize recording of refractions at near-critical distance and to provide velocity control for the near vertical reflection experiments, particularly at Moho depths to image the topography of the Moho. Along the profile, wide angle seismic reflection/refraction with 8 chemical explosions (2 tons of TNT for each) has been carried out, and 204 seismic receivers of DAS-1 & 2 models have been used to record the signals (Fig. 2). All receivers were positioned by GPS, with a station spacing of 1.5~3.0 km, depending on the topographic and tectonic complexity of the region. The acquisition system shown in Fig. 2 can

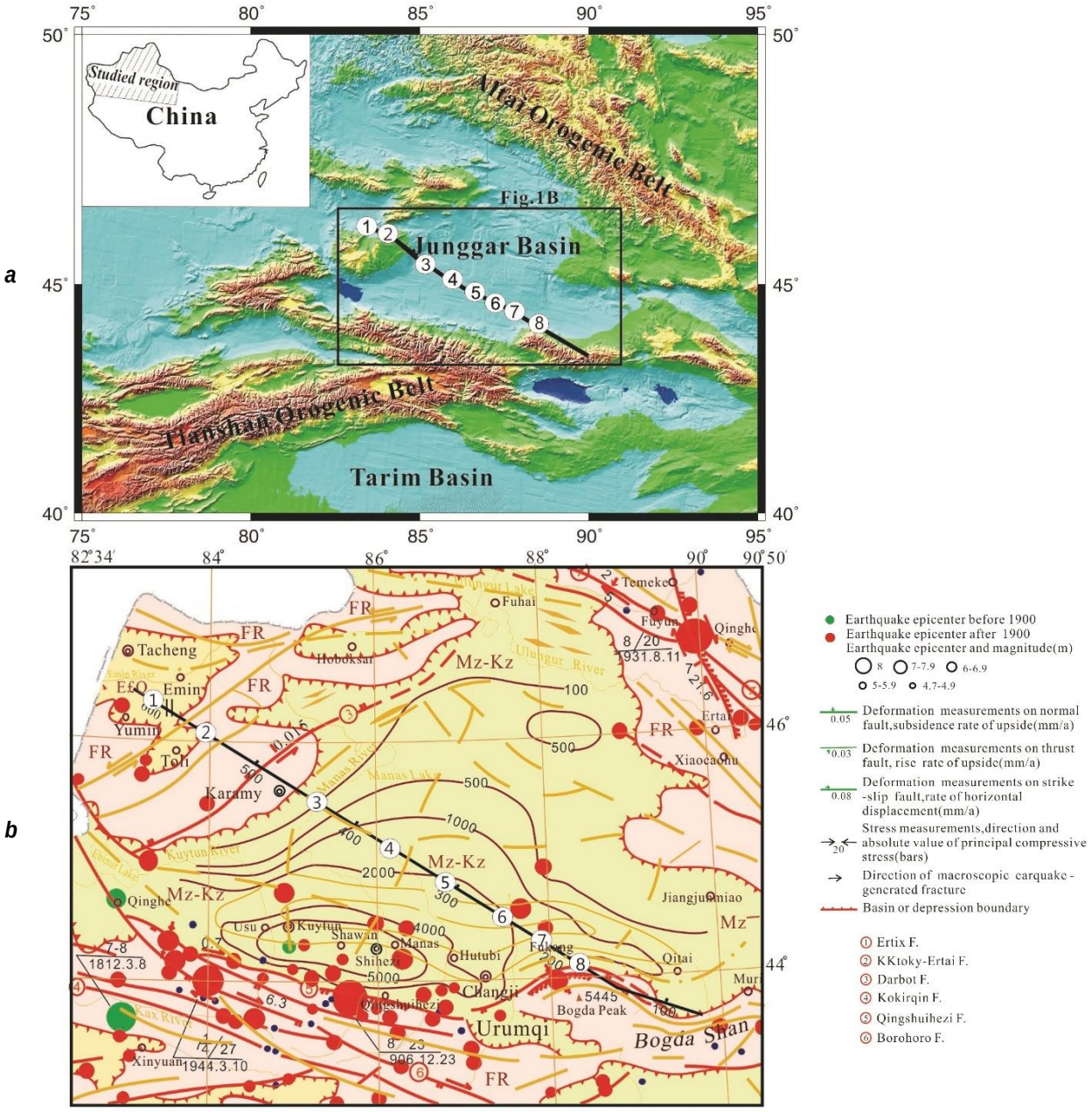

Fig. 1. Maps of the Junggar Basin:

a – topographic map of the Junggar Basin and its adjacent regions (shown is the location of about 600 km long seismic refraction / wide angle reflection profile from Emin to Qitai through the Junggar Basin; the circled numbers indicate shot points 1 to 8 of the seismic profile; the box indicates the region depicted in b);
b – the tectonic map of the target region

Рис. 1. Карты Джунгарского бассейна:

a – топографическая карта Джунгарской котловины и прилегающих районов (показано местоположение профиля сейсмического преломления / широкоугольного отражения длиной приблизительно 600 км, пересекающего Джунгарский бассейн от Эминя до Цитая; цифры в кружочках указывают очаги сейсмического взрыва профиля с 1 по 8; рамкой выделена область, изображенная на рис. b;
b – тектоническая карта целевого региона

provide us with needed coverage and seismic illumination to study the structure and properties of the basement, the structure of the crust and uppermost mantle, and some deep faults particularly those cutting up the crust and controlling the tectonic evolution of the basin. The seismic records along the profile are shown in Fig. 3. The ray tracing and theoretic seismogram are shown in Fig. 4. The effective ray coverage is shown in Fig. 5.

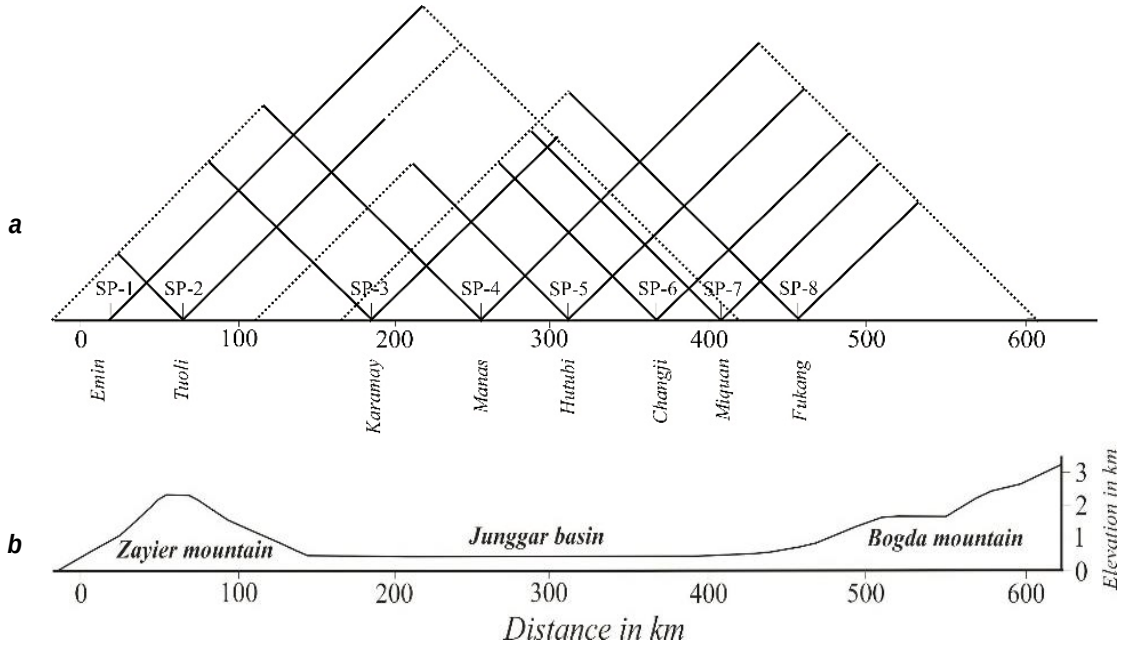

Fig. 2. Observational system (a) and elevation (b) of the seismic reflection / refraction profile from Emin to Qitai
Рис. 2. Система наблюдений (а) и высота подъема (b) профиля сейсмического отражения / преломления от Эминя до Цитая

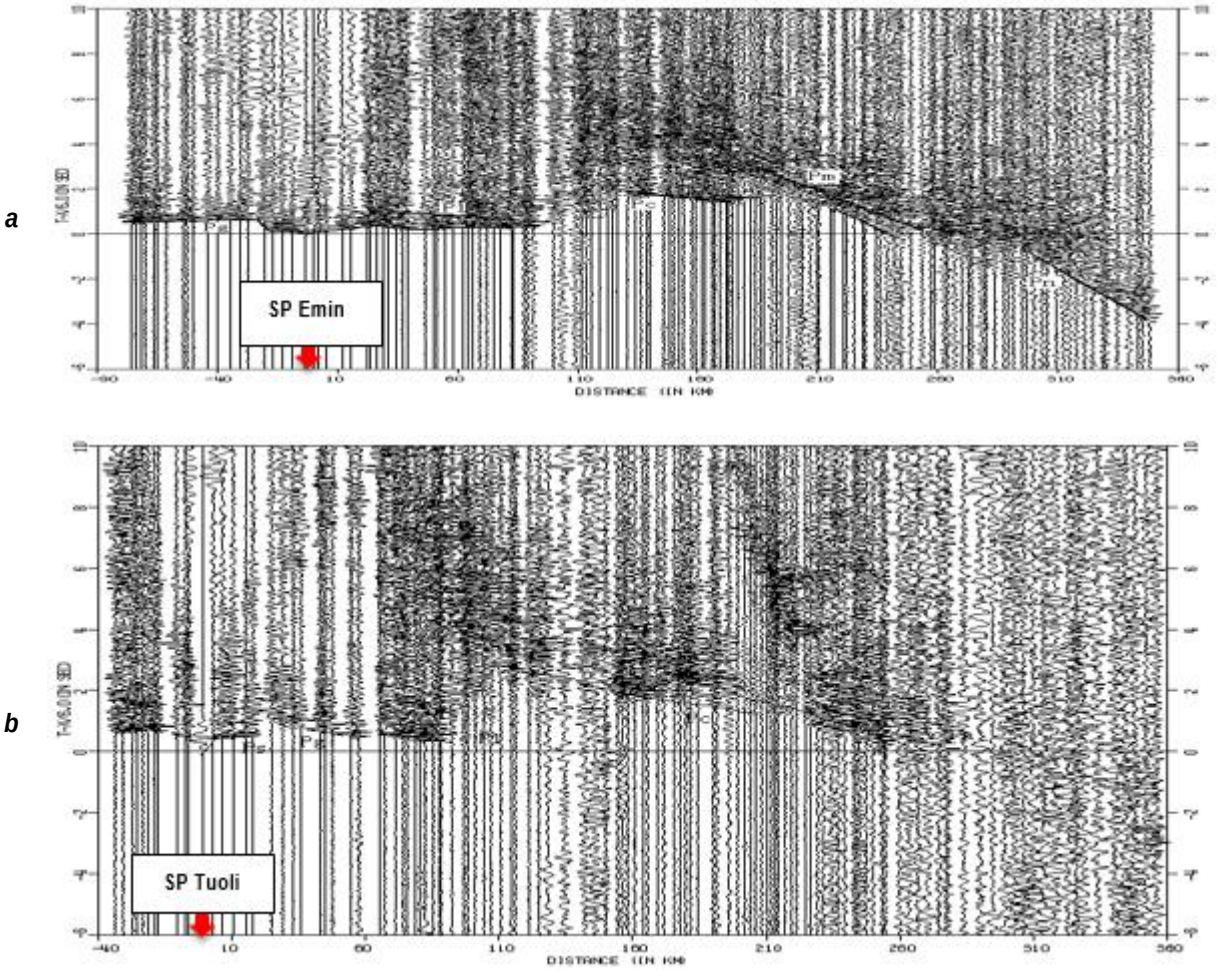

c

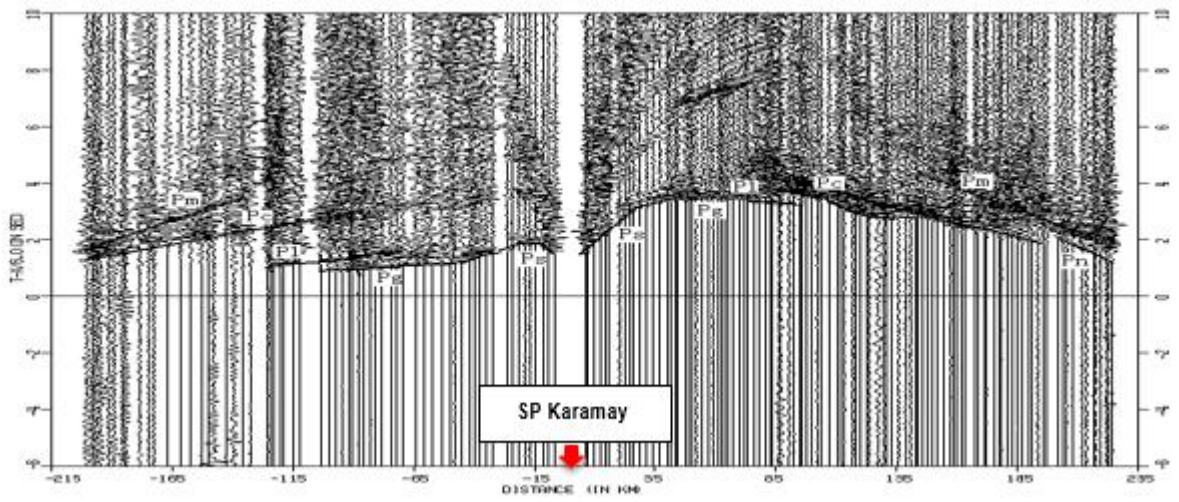
SP Karamay
DISTANCE (IN KM)

d

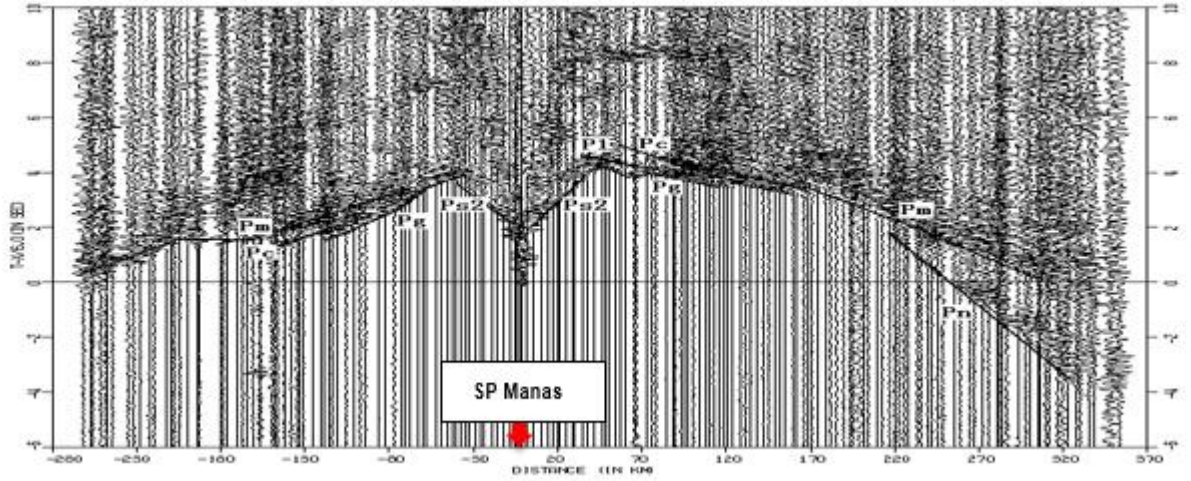
SP Manas
DISTANCE (IN KM)

e

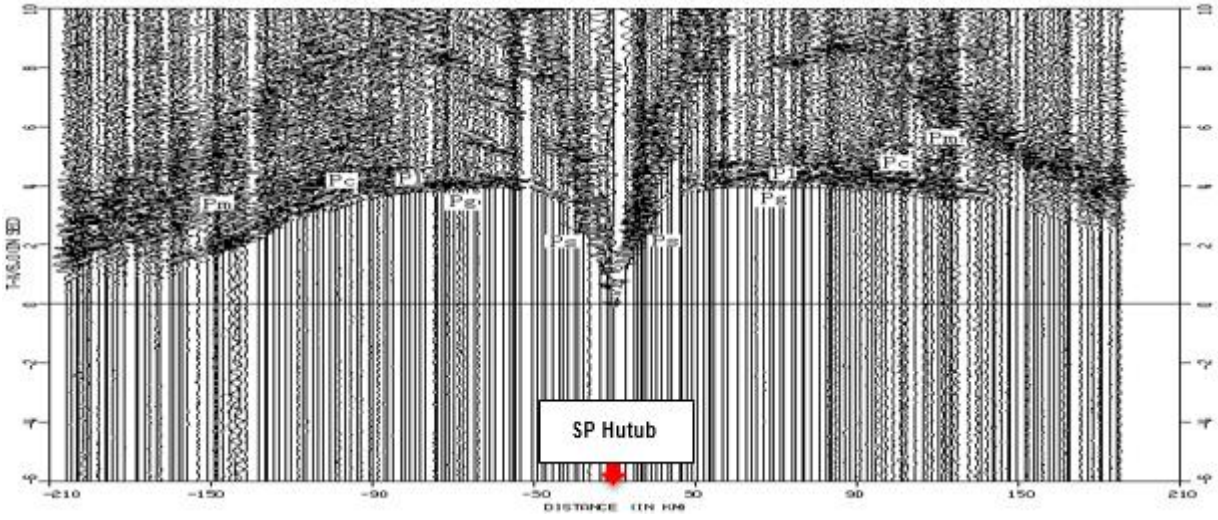
SP Hutub
DISTANCE (IN KM)

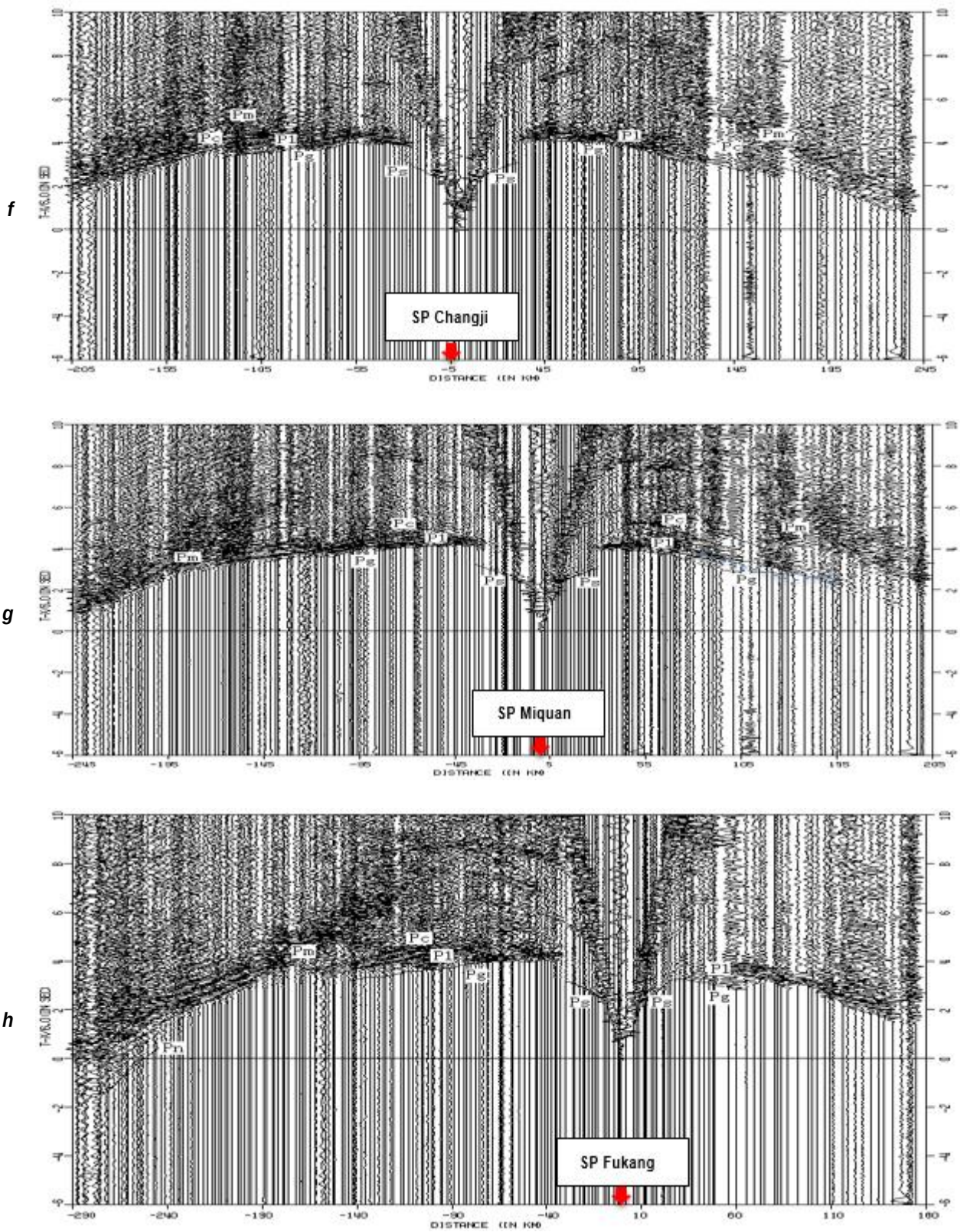

Fig. 3. Reduced seismic records:
a – at SP Emin; b – at SP Tuoli; c – at SP Karamay; d – at SP Manas;
e – at SP Hutub; f – at SP Changji; g – at SP Miquan; h – at SP Fukang
Рис. 3. Приведенные сейсмические записи
на сейсмических профилях: a – Эминь; b – Туоли; c – Карамай; d – Манас;
e – Хутуб; f – Чанцзи; g – Микван; h – Фуканг

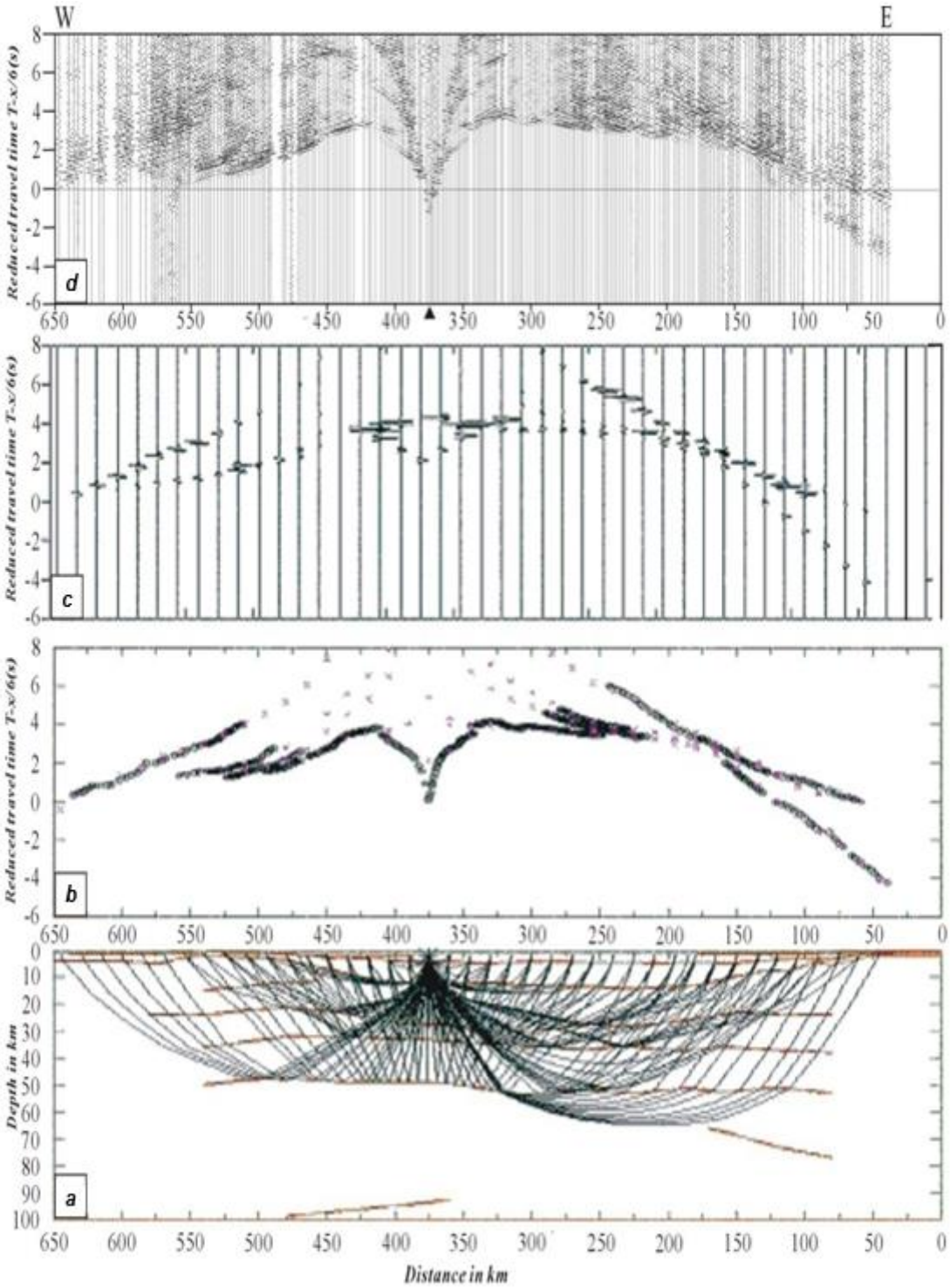

Fig. 4. Example of the ray tracing and theoretic seismogram:
a – ray tracing; b – traveling time fitting; c – amplitude fitting; d – seismic records
Рис. 4. Пример трассировки лучей и теоретической сейсмограммы:
a – трассировка лучей; b – аппроксимация времени пробега волны;
c – аппроксимация амплитуды; d – сейсмограммы

Identifying seismic phases is a key step in processing the seismic data. Due to relatively sparse shot and receiver spacing (compared with near vertical reflection), phase identification was combined with wave group (energy parcel) identification to increase accuracy. Five criteria for phase picking are listed as follows:

1) Identified phases must have connecting sections and/or connecting waves with strong amplitudes;

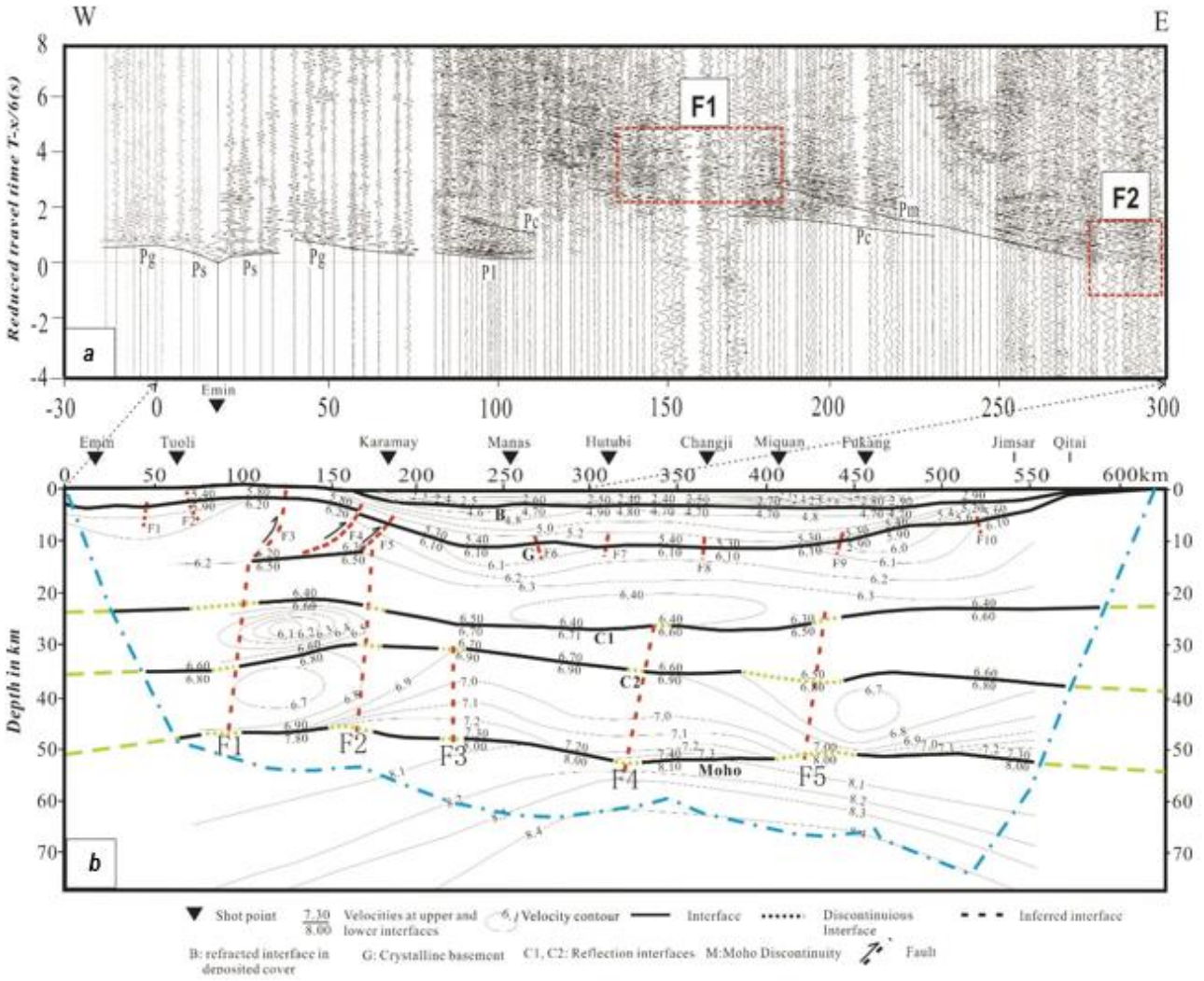

Fig. 5. The example of seismic recorders (a) and the 2D velocity structure of the crust and uppermost mantle (b) from Emin to Qitai:

a – seismic signals from SP Emin

The vertical axis indicates reduced travel time by T-x/6 in second and the horizontal axis is the distance in km from the shotpoint. The seismic recorders show strong Moho reflection along the profile but no seismic reflection from the Moho can be found at the two faults, F1 and F2, indicating that there is no wave-resistance interface at and nearby these two faults. These faults, with high seismic velocity and without obvious dislocation, are considered as the "extensional" faults, formed by north-south compression and east-west extension;

b – 2D velocity structure of the crust and uppermost mantle

The vertical axis is depth in km and the horizontal axis is distance in km. It was obtained by ray tracing and theoretical seismograms for each shot point with an improved SEIS83 program under the condition of 2D lateral inhomogeneous medium

Рис. 5. Пример сейсмических регистраторов (a) и 2D структуры скорости коры и верхней части мантии (b) от Эминя до Цитая:

a – сейсмические сигналы от СП Эминь

Вертикальная ось – это время пробега волны, уменьшенное на T-x/6 в секунду, горизонтальная ось – расстояние от очага сейсмического взрыва, км. Сейсмические регистраторы показывают сильное отражение от Мохо вдоль профиля, но в разломах F1 и F2 сейсмическое отражение от Мохо не зарегистрировано, что указывает на отсутствие границы раздела волнового сопротивления на данных разломах и рядом с ними. Обладая высокой сейсмической скоростью и не имея явной дислокации, эти разломы рассматриваются как «разломы растяжения», образованные сжатием с севера на юг и растяжением с востока на запад;

b – 2D-структура скорости земной коры и верхней мантии

По вертикальной оси отложена глубина, км, по горизонтальной оси – расстояние, км. Данные получены методом трассировки лучей и теоретических сейсмограмм для каждого очага сейсмического взрыва с использованием усовершенствованной программы SEIS83 в условиях двумерной боковой неоднородной среды

2) The amplitude of the wave must be greater than that of the noise;

3) The apparent velocity for a phase must be within a reasonable range;

4) The picked continuous travel-time curve must be greater than a minimum length;

5) Seismic reciprocity must hold for the complete observational system when we interchange the source and receiver positions.

Based on these criteria, we mainly identified the following seismic phases: Pg, P1, Pc, Pm and Pn.

(1) *Pg Wave*. Pg is a refracted wave that travels in the top part of the crystalline basement. The slope of its traveltime moveout curve yields precisely the P wave velocity in the basement. Generally, Pg can be traced to more than 130 km away from the shot point. Some significant differences in the reduced travel time for each shot point have been observed due to variations in the depth of the crystalline basement. In the Zayier Shan at the western end of the profile and Bogda Shan at the eastern end of the profile where the crystalline basements are almost exposed to the surface, the Pg wave appears much earlier (Fig. 3). However, in the middle segment of our survey line, the sediment is thick and Pg arrives much later. The apparent velocity of the Pg changes significantly at the two ends of the profile especially the transitional zones from basin to range, due to the undulation of the top surface of the crystalline basement, and changes little in the inner basin, showing that the top surface of the crystalline basement of the basin is flat. The apparent velocity of Pg is about 6.0–6.2 km/s.

(2) *P1 Wave*. The P1 wave is the reflected wave from an interface in the upper crust at a depth of 21.0–28.0 km. The amplitude and continuity of this wave changed significantly along the profile. Generally, the P1 wave is weak in energy and poor in continuity. The average velocity of the P1 wave is 5.8–6.1 km/s.

(3) *Pc Wave*. Pc is the reflected wave from the interface in the middle crust, at a depth of 36.0–40.0 km. In the Zayier Shan and the Bogda Shan, the Pc waves are weak and can be traced out to about only 40 km. In the Junggar basin, the Pc waves are relatively strong and have a good continuity. The Pc waves from Zayier Shan and Bogda Shan are different. The Pc waves from Zayier Shan (western branch of SP Karamay) are relatively strong in energy and good in continuity. It can be traced as far as 110 km, while that from the Bogda Shan is weak and poor in continuity. The variation of the amplitude and differences in average velocity are related to geological structure and material properties of each tectonic unit, distinct from the depth of the crystalline basement and undulation of the interfaces. The average velocity determined for P2 is about 6.0–6.3 km/s.

(4) *Pm Wave*. Pm is the reflected wave from the Moho discontinuity. Based on seismic records, the Pm is characterized by its clear appearance, strong amplitude, good continuity, and far-distance tracing. The Pm wave, however, has different waveforms, amplitudes and travel-time curve patterns in different sections, which suggest the existence of lateral crustal heterogeneities in different tectonic units. However, the Pm waves in the sections between 150–185 km and 220–270 km are relatively strong. This indicates that the Moho is undulated. In the basin, the Pm waves from SP Manas, SP Hutub, SP Changji and SP Fukang (western branch) have strong amplitude, excellent continuity and longer traceable distance, suggesting that the Moho of the Junggar basin is highly reflective and sharp. The average velocity of Pm waves is 6.2–6.7 km/s. However, we did not obtain a clear Pm wave from the Bogda Shan.

Even though the seismic Pm wave from the Moho in the Junggar basin is strong in energy and good in continuity, there are some sections where no clear Moho reflections have been observed (i.e., the reflectivity is very poor).

(5) *Pn Wave*. Pn is the refracted wave from the top part of the upper mantle. It can be used to determine the velocity of the uppermost mantle. Furthermore, it can be used to determine the Pm wave according to the geometric relationship between the two. Pn waves have been recorded at SP Emin (eastern branch), SP Karamay (eastern branch), SP Manas (eastern branch), SP Hutub (eastern branch) and SP Fukang (western branch) (Fig. 3). The Pn wave arrives at a source-receiver distance of approximately 200 km, with a velocity of about 8.0 km/s.

Additional wave groups P1′and Pc′were recorded and discriminated in the eastern edges

of the Zayier Shan (see SP Karamay and SP Manas) and western edge of the Bogda Shan (see SP Changji, SP Miquan and SP Fukang), indicating the existence of some additional lithologic interfaces (C1′ and Cc′) in these regions (in this notation, P1 and Pc are reflected waves from interfaces C1 and Cc in the crust). P1′ and Pc′ waves were not observed in the Junggar basin. This suggests that the crust of the Zayier Shan and Bogda Shan is more complicated than previously assumed, and provides some evidence for mantle intrusion.

Reflected and refracted waves (Pg, P_1, P_2, P_3, P_m and P_n) have been identified on different shot records and corrected from shot to shot (Fig. 3). These phases featured by high amplitudes provide a basis for dividing the crust into three velocity layers, the upper, middle and the lower crust. The first arrives at offsets of less than 70 km imply lateral variations in velocities at shallow depths (5.0 to 6.0 km/s) which can be correlated with the surface geology (Fig. 1, *b*). The velocity is estimated to be 6.2 to 6.5 km/s in the upper crust (depth of 22 to 27 km), about 6.6 to 6.7 km/s within the middle crust (~ 23 to 37 km), and 6.8 to 7.4 km/s in the lower crust (from 30 to 52 km down to the Moho). An increase in the average velocity throughout the crustal column within the crust along the profile is interpreted as an evidence for the increase in mafic content at upper crustal levels and metamorphic grade in the middle to lower crust [18, 19]. The proposed layered velocity model is non-unique but generates theoretical travel time branches that are in agree (to within ±0.1 s) with the interpreted arrivals for all of the sections.

Velocity structure of the crust and upper most mantle

Under the condition of 2D lateral inhomogeneous medium, we conducted ray tracing and constructed theoretical seismograms for each shot point with an improved SEIS83 program [22], which are presented in Fig. 4, and obtained the 2D velocity structure (Fig. 5, *b*). According to the effective ray coverage (Fig. 6), we have obtained not only the detailed velocity structure of the crust, but also that of the uppermost mantle (see the area within the blue dotted line in Fig. 5, *b*).

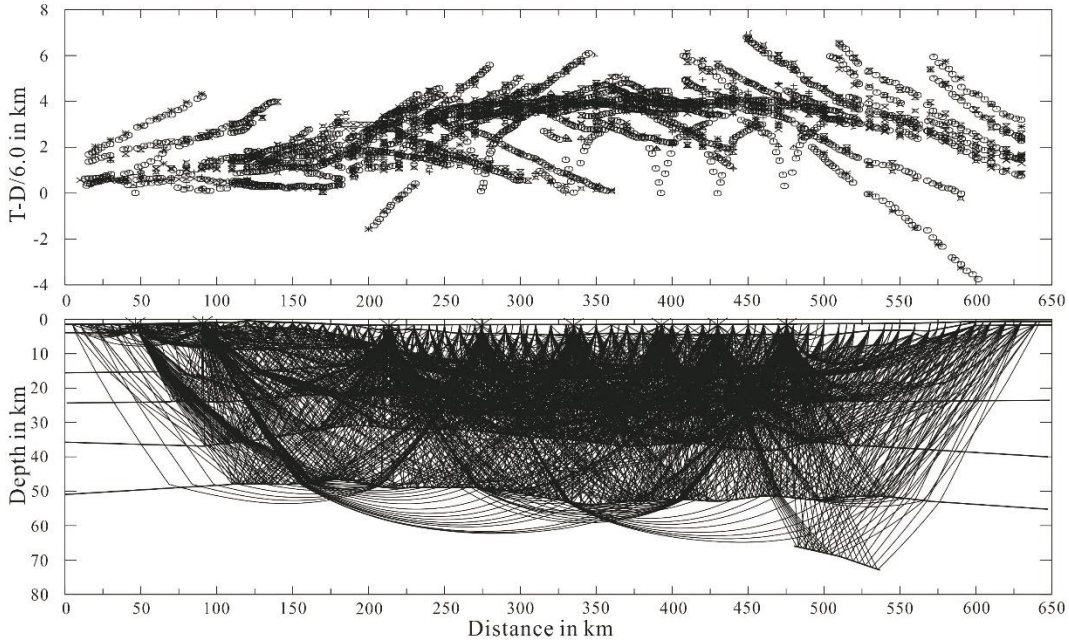

Fig. 6. Seismic ray coverage of the Emin – Qitai profile

The ray coverage of the transect is made by combining record sections of all shot points along the profile with the respective parts of the ray tracing of the corresponding shot points and deleting all calculated arrivals in the modeling which are not observed in the data

Рис. 6. Покрытие сейсмическими лучами профиля Эминь – Цитай

Покрытие поперечного разреза лучами производится путем объединения участков записи всех очагов сейсмического взрыва вдоль профиля с соответствующими частями трассировки лучей соответствующих очагов взрыва и удалением при моделировании всех вычисленных приходов волны, которые не наблюдаются в данных

Density and geomagnetic structures

Gravity and aeromagnetic data. To constrain the density structure, we need some information about the gravity. Based on the 1:200000 Bouguer gravity anomaly map of Xinjiang (Fig. 7), there are two gravity gradient zones in the northern and southern margins of the Junggar basin, which clearly delineate the shape of the basin. This is in agreement with the landscape and geological framework. The rock magnetic strength is another important factor one can use to distinguish rock types, together with the P-wave velocity and density. The aeromagnetic anomaly map of the Junggar basin shows that the southern part of the basin (Manas terrain) has a stronger magnetism than the rest of the basin.

Density and geomagnetic structures. Based on the Bouguer anomaly and aero-magnetic anomaly maps (1:200,000 scale), the 2D *P* wave velocity structure, and the faults investigated at the surface of the transect from Emil to Qitai, we constructed a model for the density structure. The starting model for the density in each cell is given by the following velocity-density relationship [23]:

$$\rho = \begin{cases} 2.78 + 0.56(V_p - 6.0) & (6.0 \geq V_p \geq 5.5) \\ 3.07 + 0.29(V_p - 7.0) & (7.5 > V_p > 6.0). \\ 3.22 + 0.20(V_p - 7.5) & (8.5 \geq V_p \geq 7.5) \end{cases}$$

Finally, the 2D density structure (Fig. 8, *a*) and magnetic intensity structure (Fig. 8, *b*) were obtained according to the Syn-Source theory and through joint inversion of gravity with geomagnetism and constrained by gravitational and geomagnetic anomalies along the profile (Fig. 7) [24].

Inference on the rock properties of the Junggar basin

According to relationships among the velocity, density and rock type (Fig. 9) [25], and based on the velocity distribution along the profile from Xayar to Burjing [21] and from Baicheng to Da Qaidam [19], basement rock types of the Junggar basin were identified and catalogued (Table).

The velocity is obtained from seismic data generated by artificial earthquakes, and the density and geomagnetic intensity are determined by joint inversion of gravity with geomagnetism along the same profile. The results suggest that the basement lithology of the Junggar basin is complicated especially towards its center. It is composed of mafic, ultra-mafic, and acidic rocks, such as granite, schist, granulite, gabbro.

Moreover, the Pb [23, 26, 27], Nd, and Sr [28] isotope compositions of post-collisional intermediate and acidic plutons in the Junggar basin show that these plutons originated from

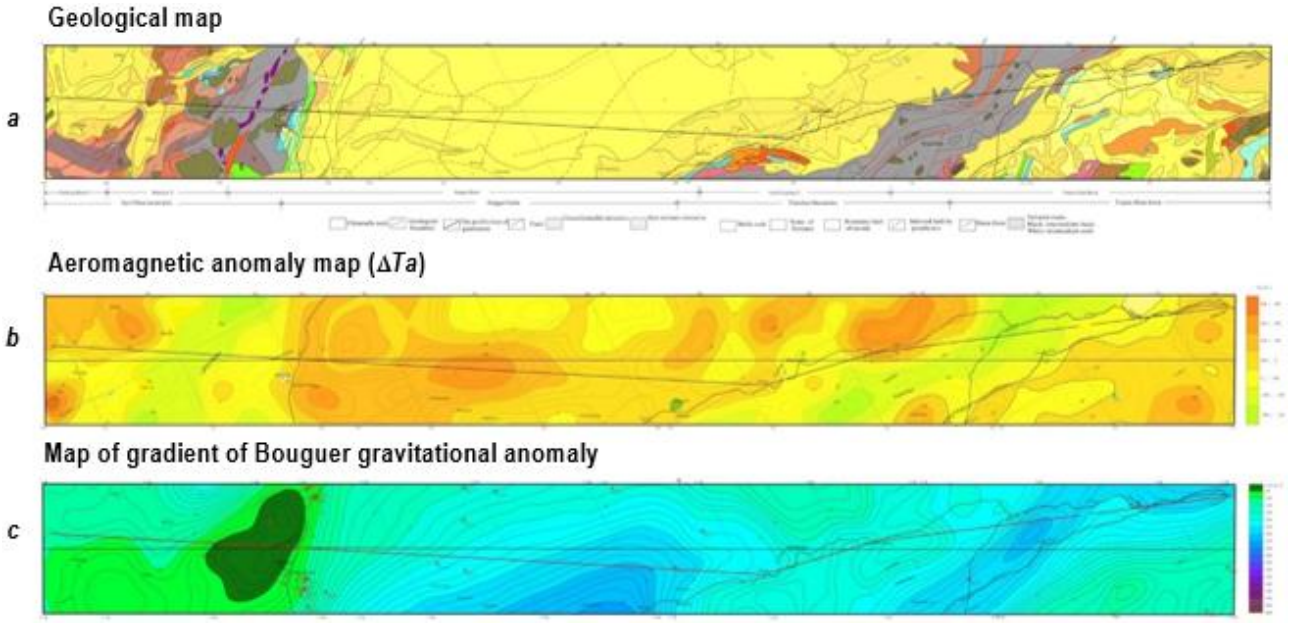

Fig. 7. The map showing geology (a), geomagnetism (b) and gravitation (c) along the profile
Рис. 7. Карта геологии (a), геомагнетизма (b) и гравитации (c) вдоль разреза

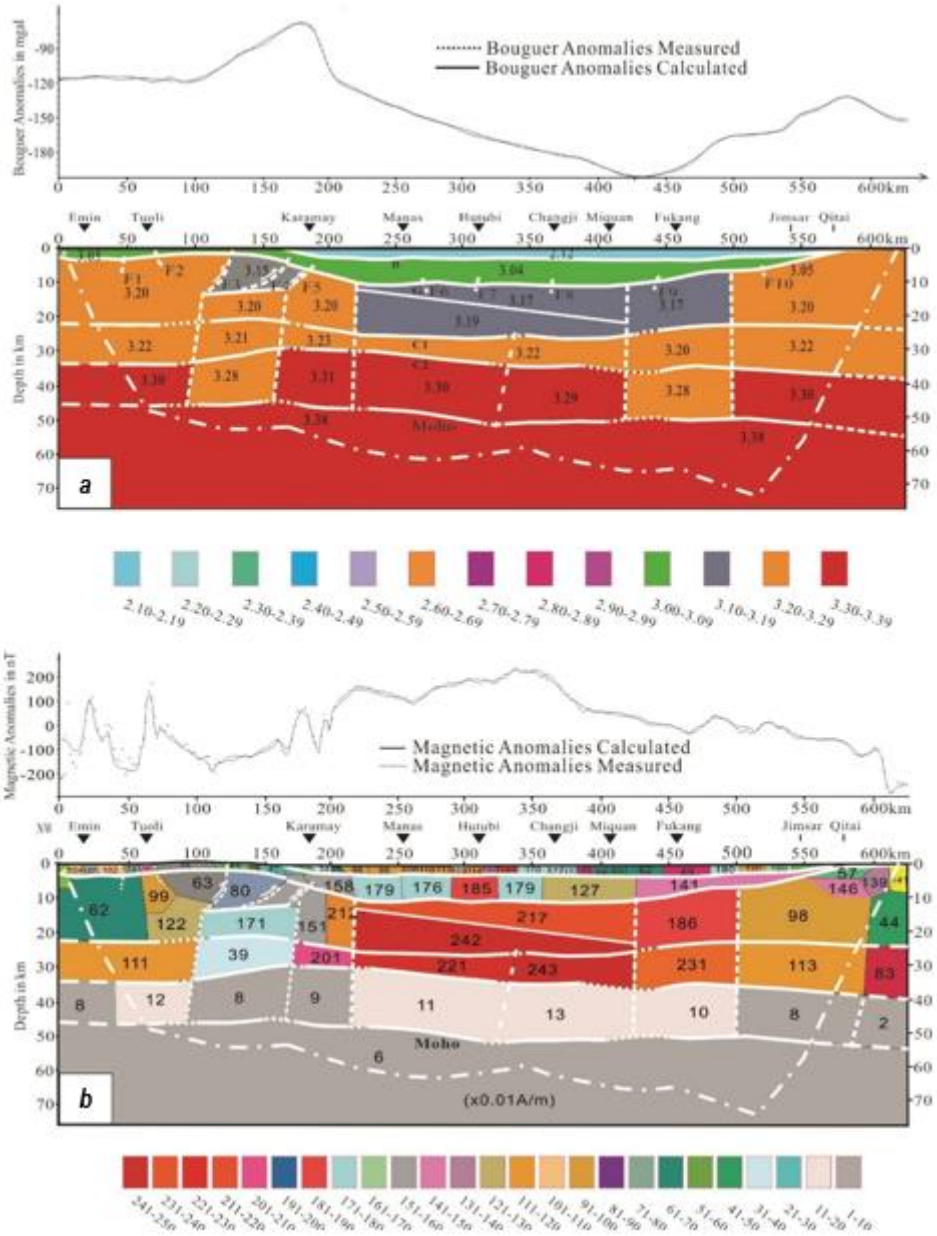

Fig. 8. The density (a) and magnetic intensity (b) of the crust and upper most mantle along the profile from Emin to Qitai

The initial density model was designed based on the relation between velocity and density. The density and magnetic intensity were obtained by joint inversion of the gravity and geomagnetic anomaly based on the Syn-Source principle of gravity and geomagnetism. The upper panel of the a is Bouguer's anomaly measured and calculated by fitting. The lower panel is the density in g/cm^3. It was obtained by forward modeling under a same frame obtained by velocity structure for both the density and magnetic intensity. The upper panel of the b is magnetic anomaly measured and calculated by fitting. The lower panel is the magnetic intensity in 0.01·A/m obtained by the same way as the density modeling. For the detail description of the joint inversion, please see [24]

Рис. 8. Плотность (а) и магнитная напряженность (b) коры и верхней части мантии по профилю от Эминя до Цитая

Первоначальная модель плотности была разработана на основе соотношения между скоростью и плотностью. Плотность и магнитная интенсивность были получены совместной инверсией гравитационной и геомагнитной аномалии на основе принципа Syn-Source гравитации и геомагнетизма. В верхней части рис. а представлена аномалия Буге, измеренная и рассчитанная путем аппроксимации. Нижняя часть рис. а показывает плотность, г/см^3. Данные были получены прямым моделированием в той же системе отсчета, полученной с помощью структуры скорости, как для плотности, так и для магнитной напряженности. Верхняя часть рис. b демонстрирует магнитную аномалию, измеренную и рассчитанную путем аппроксимации. Нижняя часть рис. b показывает магнитную напряженность, 0.01·A/m, полученную тем же способом, что и при моделировании плотности. Подробное описание совместной инверсии см. в [24]

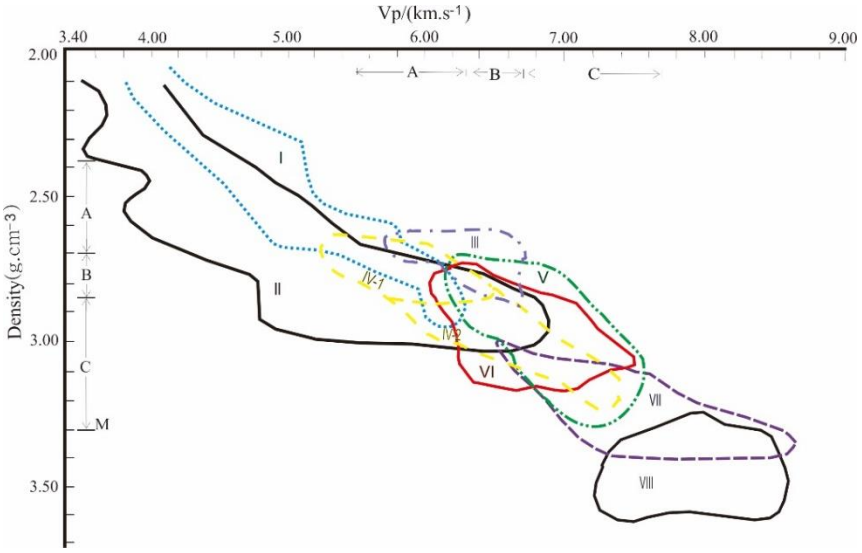

Fig. 9. Relationship among density, velocity and properties of various rocks at depth (after Liu et al. [25])
I – sandstone; II – basalt; III – granite; IV-1 – neutral to acid schist or gneiss; IV-2 – neutral to basic schist or gneiss; V – granulite; VI – gabbro; VII – peridotite; VIII – eclogite; A – upper crust; B – middle crust; C – lower crust

Рис. 9. Взаимосвязь между плотностью, скоростью и свойствами различных пород на глубине (по Лю и др. [25])
I – песчаник; II – базальт; III – гранит; IV-1 – от нейтрального до кислого сланца или гнейса; IV-2 – от нейтрального до основного сланца или гнейса; V– гранулит; VI – габбро; VII – перидотит; VIII – эклогит; А – верхняя кора; Б – средняя кора; С – нижняя кора

Basement parameters along the Emin – Qitai profile
Параметры фундамента по профилю Эминь – Цитай

Range	0–135	135–160	160–210	210–250	250–355	355–405	405–445	445–540	540–610
Velocity	6.10	6.15	6.25	6.30	6.17	6.30	6.30	6.17	6.15
Density	2.65	2.65	2.65	2.74	2.65	2.65	2.65	2.65	2.65
Mag-intensity	62–120	62–72	75–122	80–135	151–179	176	180	127	141
Rock	Granite	Granite	Granite	Granite, schist, granulite, gabbro	Granite	Granite	Granite	Granite	Granite

the sub-oceanic mantle and not from a craton continental basement. No known Precambrian strata have yet been discovered around the basin. However, Paleozoic oceanic rocks and relic oceanic sediments of the middle Paleozoic age are widely distributed. To the south of the Karamay fault the paleocurrent is directed to the north as shown by imbricated clasts and groove marks in turbidities of continental shelf facies from the Silurian age. This also suggests that the provenance of these strata were pre-Silurian continental blocks. Furthermore, the provenances were probably not the small blocks made up of mafic volcanic rocks that date to the Ordovician or Cambrian ages [12].

The aeromagnetic anomaly of the Junggar basin shows that the southern part of the basin (Manas terrane) has much stronger magnetism, which is in agree with the magnetization of Precambrian schist, migmatites, granites, and hornblende schist. However, the results of joint inversion of gravity with aeromagnetism show that these high aeromagnetic anomalies may be produced by ancient blocks or the NNE trending faults resulting from modern north-south compression. These faults potentially provide channels for deep material to move up into the crust, and subsequently intrude laterally into different sub-layers of crust. This would change the contents of the Junggar basement, resulting in the higher average velocity, density, and magnetism observed in the crust of the basin. These intrusions may have originated as oceanic basalt and tholeiite. Based on the 1:200000 gravity

anomaly map of Xinjiang [29], there are two gravity gradient zones in the northern and southern margins of the Junggar basin, which clearly delineate the shape of basin. This is in agreement with the landscape and geological framework. The 2-D velocity and density structures along the Xayar-Burjing profile indicate that the crustal thickness is about 47 km in the Junggar basin. This thickness however, includes the 15 km thick sediments that have accumulated since the Devonian era. The thickness of the Mesozoic and Cenozoic sediments alone is greater than 11 km. Not taking into account the sediments, the crustal thickness of the crystalline basement of the Junggar basin is only 32 km. The 2-D density structure of the Xayar-Burjing profile [21] shows that the density of the basement roof of the Junggar basin is different in the Wulungu and Manasi terrains; the density and velocity of the former is 2.87 g/cm^3 and 5.9 km/s, while that of the latter is about 2.85 g/cm^3 and 5.8 km/s.

Geological Interpretation

Based on the 2D velocity (Fig. 5, *b*), 2D density (Fig. 8, *a*) and 2D magnetic intensity (Fig. 8, *b*), and combined with geological and geochemical analysis [8] we developed a final model as Fig. 10.

Vertically, the crust is composed of three layers: the upper, middle and lower crust, bottomed by the C1, C2 and Moho interfaces, respectively. The upper layer of the upper crust consists the deposited cover bottomed by the interface G, and the lower layer bottomed by the interface C1. The sedimentary cover ranges in thickness from 1 km to 12 km and reaches a maximum depth of 12 km, while the crystalline basement ranges in thickness from approximately 12 km to 20 km and reaches a maximum depth of ~ 30 km. The velocity in the deposited cover undergoes large lateral variations, especially near Karamay, Hutub and Fukang (Fig. 5). In addition, the density and the magnetic intensity also change greatly (Fig. 8). The crystalline basement exhibits high velocity zones, including a region near Hutub, at ~ 20 km depth, where velocities are 0.1~0.2 km/s higher than surrounding medium, and so as the density and geomagnetic intensity.

The middle crust, defined by the interfaces C_1 and C_2, is comparatively thin, with thicknesses ranging from 4 km to 15 km and a maximum depth of 37 km. Slight variation occurs on velocity, except for a low velocity zone beneath Karamay and Fukang, where the corresponding density is low. The middle crust has a dumbbell shape, i.e. thin in the middle and thick at the two ends of the profile.

Obvious lateral variations are obtained in the lower crustal velocity. The most complex regions lay beneath the Karamay and Fukang, which are two active tectonic zones in the Junggar basin[1]. Here, two low velocity zones with low densities have developed, near which developed several faults cutting up the crust. The lower crust is further characterized by uniform thickness of roughly 15 km, despite having heterogeneous composition [21]. The crustal thickness of the Junggar basin ranges from 46 to 56 km.

Below the Moho interface, the uppermost mantle of the Junggar basin varies in shape of the velocity contours. The contours at the uppermost mantle are convex, indicating that the velocity is higher at the center of the basin than that at its either side [30]. It may further suggest that the upper mantle material may inject into the crust of the Junggar basin, because of the similar rock distribution along the profile (Fig. 10, Table). The Earth's topography at short wavelengths results from active tectonic processes, whereas at long wavelengths it is largely determined by isostatic adjustment for the density and thickness of the crust [30].

On these interfaces, we found several sections from which the seismic waves are very weak, indicating a lower reflection coefficient (Fig. 3). This may reflect the presence of deep faults, which could be confirmed by the combined results of seismic velocity (wide angle reflection/refraction profiling, (Fig. 5), density, geomagnetic intensity (joint inversion of gravity with aeromagnetism (Fig. 8), P-wave imaging[2] and seismic converted wave profile crossing the northern part of the basin [24]. All these faults, with little reflectivity and no obvious dislocation,

[1] Xu Y. Seismic tomography for northwestern China and its tectonic implication: Ph.D dissertation. Institute of Geophysics, CAS, 1999.
[2] Ibid.

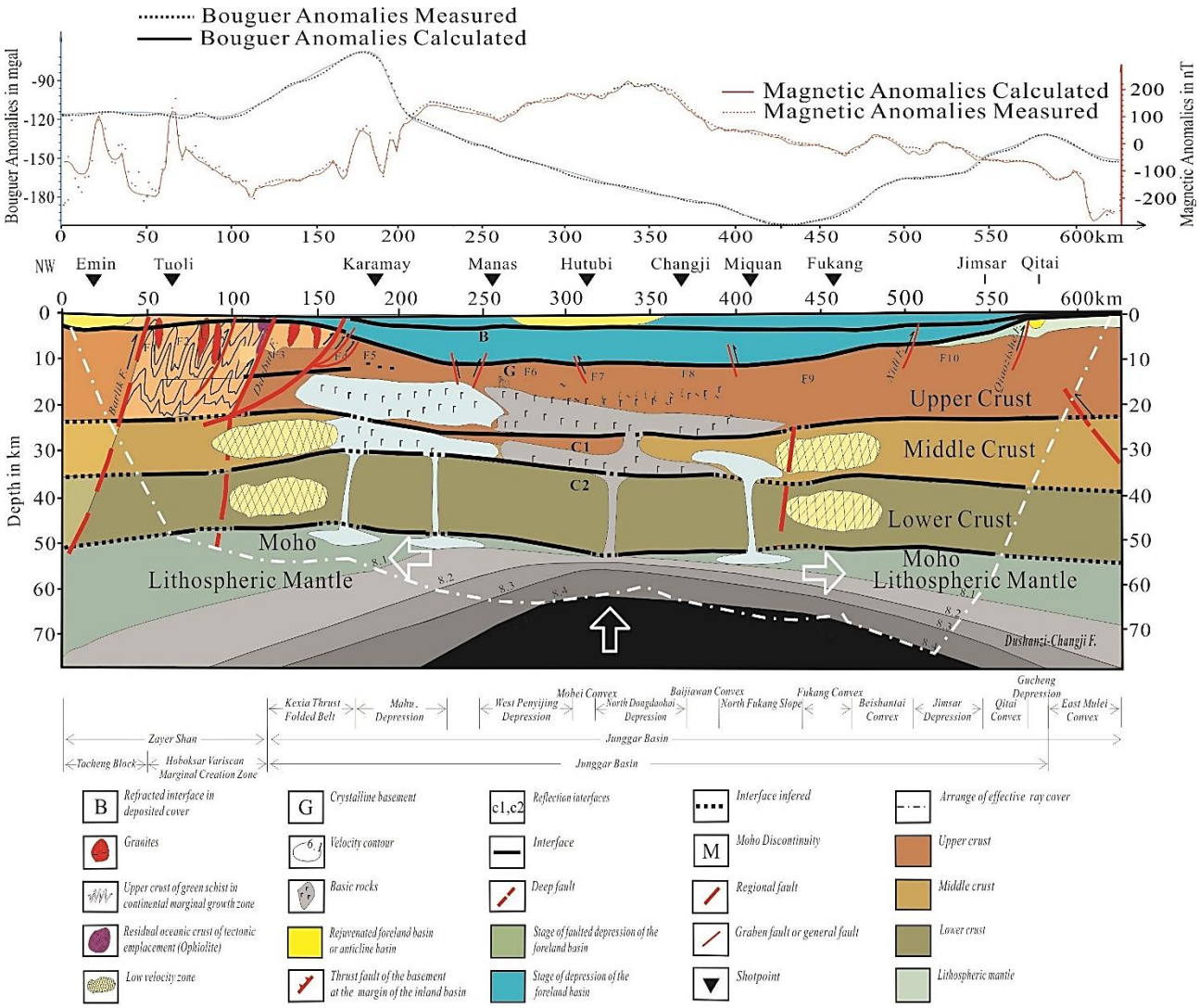

Fig. 10. The geological interpretation of the profile from Emin to Qitai

The upper panel shows the gravitational and geomagnetic anomalies measured and calculated by fitting. The lower panel with the geological background and the legend below it shows the geological interpretation of the profile from Emin to Qitai, based on the 2D velocity structure, 2D density structure and 2D magnetic intensity structure, and combined with geological and geochemical analysis. The black triangles indicate shot points. Along a ~ 600 km long transect from Emin to Qitai developed several N-S trending blind faults, which are located at the lower part of the upper crust, the middle crust and the lower crust and cut up the Moho. These faults, with high seismic velocity and without obvious dislocation, are considered as "extensional" faults, formed by north-south compression and east-west extension. These deeply rooted faults provide channels for basic to ultra-basic rocks from upper mantle migrating into the crust and mixed up with the crustal material, causing the crust of the basin with thin thickness, high seismic velocities, high densities and high magnetic intensities

Рис. 10. Геологическая интерпретация профиля от Эминя до Цитая

В верхней части рисунка показаны гравитационные и геомагнитные аномалии, измеренные и рассчитанные при помощи аппроксимации. В нижней части, где показан геологический фон и даны условные обозначения, дается геологическая интерпретация профиля от Эминя до Цитая на основе 2D-структуры скорости, 2D-структуры плотности и 2D-структуры магнитной напряженности в сочетании с геологическим и геохимическим анализом. Черные треугольники обозначают очаги сейсмического взрыва. Вдоль поперечного разреза длиной ~ 600 км от Эминя до Цитая сформировалось несколько слепых разломов простиранием с севера на юг, которые расположены в нижней части верхней коры, в средней части коры и в нижней коре и разрезают Мохо. Обладая высокой сейсмической скоростью и не имея видимых дислокаций, эти разломы рассматриваются как «разломы растяжения», образованные сжатием с севера на юг и растяжением с востока на запад. Эти глубокие разломы обеспечивают каналы для мигрирования основных и ультраосновных пород из верхней мантии в кору, где они смешиваются с материалом земной коры, в результате чего кора бассейна становится тонкой, приобретает высокие сейсмические скорости, высокую плотность и высокую магнитную напряженность

are considered as “extension” faults. They developed with a high angle in the middle and lower crust and extended upwards into the lower parts of upper crust. They were formed probably by the collision of the Junggar basin with the Tarim basin at the end of Permian [21].

Horizontally, the southern Junggar basin along the profile can be divided into three sections, which are the western section (0–150 km), the central section (150–420 km) and the eastern section (420–600 km), based on the velocity, the density and geomagnetic structures (Fig. 8). In the western section, i.e. the western mountain area, the tectonic activities are more active, where developed many faults. The velocity distribution is complicated with several low velocity zones formed in the middle crust and lower crust, respectively. The densities in the low velocity zone are lower, but the magnetic intensities are complex, featured by high frequency of geomagnetic anomalies. In the central section, mostly the Junggar basin, the velocity, the density and geomagnetic intensity are consistently high, especially in the lower part of the upper crust and the middle crust. In this section, the Moho interface sinks down and the uppermost mantle uplifted. In the eastern part of our profile, the velocity, the density and geomagnetic intensity are relatively low at the eastern margin of the basin, with two lower velocity zones developed in the middle and lower crust, respectively.

Geologically, the evolution of the Tianshan Orogen and Junggar basin can be divided into several stages: the early Paleozoic intra-oceanic arc evolution, the Early Devonian and later Middle Devonian rifting evolution of the Junggar ocean, formed from the rifting of the early Paleozoic folded basement, the relic ocean from Later Devonian to late Carboniferous, and the final accretion orogeny in the late Carboniferous-early Permian [8]. We infer that this final accretion orogeny in the late Carboniferous-early Permian was so strong that some deep faults with S-N direction were formed by S-N compression and E-W extension. In such process, the hot materials from upper mantle migrated to the crust through the deep faults and mixed up with the crustal materials in the central basin, which could be further approved by the high velocity, high density and high geomagnetic intensity beneath the basin. The two low velocity zones at both sides of the basin may be attributed to the heat from upper mantle.

The exchange of the materials or energy of the uppermost mantle with those in the crust is manifested by the heat evolution of the basin. Based on the heat flow variations of the basins in northwestern China since Paleozoic time [31], the heat flow of the Junggar basin since Carboniferous-Permian reduced gradually from 120~150 $mW.m^{-2}$ to 52 $mW.m^{-2}$ at present, while that of the Tarim basin, the Qaidam basin and the Sichuan basin almost keep the same value of 45 $mW.m^{-2}$, even with a tendency of increase. Therefore, we infer that the high heat value of the Junggar basin may have been caused by the hot materials from the upper mantle mixing the crystalline basement of the Junggar basin.

References

1. Kamen-Kaye M, Meyerhoff AA, Taner I. Junggar basin: a Permian to Cenozoic intermontane complex in northwestern China. *Senckenbergiana Lethaea*. 1988;69 (3-4):289–313.

2. Li D, He D, Lian Y, Lu Y, Yi Z. Structural evolution and late Carboniferous magmatism of the Zhongguai arc in the western Junggar Basin, Northwest China: implications for tectonic evolution of the Junggar Ocean. *International Geology Review*. 2017;59(10):1234–1255. https://doi.org/10.1080/00206814.2016.1160801

3. Yan W, Wang G, Li L, Zhang L, Yu J, Yang G, et al. Deformation analyses and their geological implications of Carboniferous-Permian tectonic transition period in northwest margin of Junggar basin. *Earth Science*. 2015;40(3):504–520. (In Chinese) https://doi.org/10.3799/dqkx.2015.040

4. Carroll AR, Liang Y, Graham SA, Xiao X, Hendrix MS, Chu J, et al. Junggar basin, northwest China: trapped Late Paleozoic ocean. *Tectonophysics*. 1990;181(1-4):1–14.

5. Wang Y, Mooney WD, Yuan X, Coleman RG. The crustal structure from the Altai Mountains to the Altyn Tagh fault, northwest China. *Journal of Geophysical Research: Solid Earth*. 2003;108(B6):1–16. https://doi.org/10.1029/2001JB000552

6. Wu S, Huang R, Xu Y, Yang Y, Jiang X, Zhu L. Seismological evidence for a remnant oceanic slab in the western Junggar, Northwest China. *Journal of Geophysical Research: Solid Earth*. 2018;123(5):4157–4170. https://doi.org/10.1029/2017JB015332

7. Zhang S, Xu Y, Jiang L, Yang B, Liu Y, Griffin WL, et al. Electrical structures in the northwest margin of the Junggar basin: Implications for its late Paleozoic

geodynamics. *Tectonophysics*. 2017;717:473–483. https://doi.org/10.1016/j.tecto.2017.08.031

8. Xiao W, Windley BF, Sun S, Li J, Huang B, Han C, et al. A tale of amalgamation of three Permo-Triassic Collage systems in Central Asia: oroclines, sutures, and terminal accretion. *Annual Review of Earth and Planetary Sciences*. 2015;43:477–507. https://doi.org/10.1146/annurev-earth-060614-105254

9. Wu Q. Structural evolution and oil prospecting in Wuqingfu-1 Junggar Basin. *Geology of Xinjiang*. 1986;4(3):1–9.

10. You Q. Geotectonic unit division and hydrocarbon-bearing property of each tectonic stage in Junggar Basin of Youqimei. In: Wang Y. (ed.). *Petroleum geology of Junggar Basin comprehensive research*. Lanzhou: Gansu Science and Technology Publishing House, 1992. p.114–221.

11. Zhao B. Formation and evolution of Zhaobai 1 Junggar Basin. *Petroleum Geology of Xinjiang*. 1992;13(3):191–196.

12. Xiao X, Tang Y, Feng Y, Zhu B, Li J, Zhao M. *Tectonic evolution of the northern Xinjiang and its adjacent regions*. Beijing: Geological Publishing House; 1992. 169 p. (In Chinese)

13. Yang W, Kuang J, Xu C. Formation conditions and prediction of large oilfields in Junggar Basin. *Petroleum Geology of Xinjiang*. 1995;16(3):2101–2111.

14. Sun Z. Mesozoic-Cenozoic foreland basins in central and Western China and their hydrocarbon potential. *Gas Geology*. 1998;4(3):16–301.

15. Zhang Z, Liou J, Coleman RG. An outline of the plate tectonics of China. *Geological Society of America Bulletin*. 1984;95(3):295–312. https://doi.org/10.1130/0016-7606(1984)95<295:AOOTPT>2.0.CO;2

16. Hsü KJ. Relict back-arc basins: principles of recognition and possible new examples from China. In: Kleinspehn KL, Paola C (eds.). *New perspectives in basin analysis*. New York: Springer; 1988. p.245–263.

17. Argand E. La tectonique de l'Asie. *Proc. 13th Int. Geol. Congr*. 1924;1(5):170–372.

18. Mooney WD, Prodehl C, Pavlenkova NI. Seismic velocity structure of the continental lithosphere from controlled source data (Chapter 54). In: Lee WHK, Kanamori H, Jennings PC, Kisslinger C (eds.). *International handbook of earthquake & engineering seismology*. Part A. International Geophysics Series. Vol. 81A. Amsterdam – Boston – London – New York: Academic Press; 2002. p.887–910.

19. Zhao J, Mooney WD, Zhang X, Li Z, Jin Z, Okaya N. Crustal structure across the Altyn Tagh Range at the northern margin of the Tibetan plateau and tectonic implications. *Earth and Planetary Science Letters*. 2006;241(3-4):804–814. https://doi.org/10.1016/j.epsl.2005.11.003

20. Zhao J, Jin Z, Mooney WD, Okaya N, Wang S, Gao X, et al. Crustal structure of the central Qaidam basin imaged by seismic wide-angle reflection / refraction profiling. *Tectonophysics*. 2013;584:174–190. https://doi.org/10.1016/j.tecto.2012.09.005

21. Zhao J, Liu G, Lu Z, Zhang X, Zhao G. Lithospheric structure and dynamic processes of the Tianshan orogenic belt and the Junggar basin. *Tectonophysics*. 2003;376(3-4):199–239. https://doi.org/10.1016/j.tecto.2003.07.001

22. Červený V, Molotkov IA, Pšenčík I. *Ray method in seismology*. Prague: University Karllova; 1977. 214 p.

23. Feng R, Yan H, Zhang R. The method of quick inversion for 3D potential field and program designing. *Journal of Geology*. 1986;4:390–402.

24. Zhao J. *Geodynamic conditions for northern margin of Tibetan Plateau*. Beijing: Science Press, 2012.

25. Liu Y, Wu X. Wave velocity in rocks under high temperature and pressure and composition of the deep crust. *Chinese Journal of Geophysics*. 1997;40(3):211–220. (In Chinese)

26. Tilton GR, Kwon ST, Coleman RG, et al. Isotoic studies from the west Junggar Mts, NW China. *Geological Society of America, Abstracts with Programs*. 1986;18.

27. Xiao X, Tang Y, Li J, Jhu B. On the tectonic evolution of the northern Xinjiang, Northwest China. *Xianjiang Geological Science*. 1990;1:47–68. (In Chinese)

28. Hopson C, Wen J, Tilton G, Tang Y, Zhu B, Zhao M. Paleozoic plutonism in east Junggar, Bogdashan, and eastern Tianshan, NW China. *EOS, Transactions, American Geophysical Union*. 1989;70:1403–1404.

29. Zhao J, Li Z, Cheng H, Yao C, Li Y. Structure of lithospheric density and geomagnetism beneath the Tianshan orogenic belt and their geodynamic implacations. *Chinese Journal of Geophysics*. 2004;47(6):1061–1067.

30. Mooney WD, Vidale JE. Thermal and chemical variations in subcrustal cratonic lithosphere: evidence from crustal isostasy. *Lithos*. 2003;71(2-4):185–193. https://doi.org/10.1016/j.lithos.2003.07.004

31. Wang F, Yang M, Zheng J. Geochemical evidence of the basement assembled by island arc volcanic terranes in Junggar basin. *Acta Petrologica et Mineralogica*. 2002;21(1):1–10. (In Chinese)

Список литературы

1. Kamen-Kaye M., Meyerhoff A.A., Taner I. Junggar basin: a Permian to Cenozoic intermontane complex in northwestern China // Senckenbergiana Lethaea. 1988. Vol. 69. Iss. 3-4. P. 289–313.

2. Li D., He D., Lian Y., Lu Y., Yi Z. Structural evolution and late Carboniferous magmatism of the Zhongguai arc in the western Junggar Basin, Northwest China: implications for tectonic evolution of the Junggar Ocean // International Geology Review. 2017. Vol. 59. Iss. 10. P. 1234–1255. https://doi.org/10.1080/00206814.2016.1160801

3. Yan W., Wang G., Li L., Zhang L., Yu J., Yang G., et al. Deformation analyses and their geological implications of Carboniferous-Permian tectonic transition period in northwest margin of Junggar basin // Earth Science. 2015. Vol. 40. Iss. 3. P. 504–520. https://doi.org/10.3799/dqkx.2015.040

4. Carroll A.R., Liang Y., Graham S.A., Xiao X., Hendrix M.S., Chu J., et al. Junggar basin, northwest China: trapped Late Paleozoic ocean // Tectonophysics. 1990. Vol. 181. Iss. 1-4. P. 1–14.

5. Wang Y., Mooney W.D., Yuan X., Coleman R.G. The crustal structure from the Altai Mountains to the Altyn Tagh fault, northwest China // Journal of Geophysical Research: Solid Earth. 2003. Vol. 108. Iss. B6. P. 1–16. https://doi.org/10.1029/2001JB000552

6. Wu S., Huang R., Xu Y., Yang Y., Jiang X., Zhu L. Seismological evidence for a remnant oceanic slab in the western Junggar, Northwest China // Journal of Geophysical Research: Solid Earth. 2018. Vol. 123. Iss. 5. P. 4157–4170. https://doi.org/10.1029/2017JB015332

7. Zhang S., Xu Y., Jiang L., Yang B., Liu Y., Griffin W.L., et al. Electrical structures in the northwest margin of the Junggar basin: Implications for its late Paleozoic geodynamics // Tectonophysics. 2017. Vol. 717. P. 473–483. https://doi.org/10.1016/j.tecto.2017.08.031

8. Xiao W., Windley B.F., Sun S., Li J., Huang B., Han C., et al. A tale of amalgamation of three Permo-Triassic Collage systems in Central Asia: oroclines, sutures, and terminal accretion // Annual Review of Earth and Planetary Sciences. 2015. Vol. 43. P. 477–507. https://doi.org/10.1146/annurev-earth-060614-105254

9. Wu Q. Structural evolution and oil prospecting in Wuqingfu-1 Junggar Basin // Geology of Xinjiang. 1986. Vol. 4. Iss. 3. P. 1–9.

10. You Q. Geotectonic unit division and hydrocarbon-bearing property of each tectonic stage in Junggar Basin of Youqimei // Petroleum geology of Junggar Basin comprehensive research / ed. Y. Wang. Lanzhou: Gansu Science and Technology Publishing House, 1992. P. 114–221.

11. Zhao B. Formation and evolution of Zhaobai 1 Junggar Basin // Petroleum Geology of Xinjiang. 1992. Vol. 13. Iss. 3. P. 191–196.

12. Xiao X., Tang Y., Feng Y., Zhu B., Li J., Zhao M. Tectonic evolution of the northern Xinjiang and its adjacent regions. Beijing: Geological Publishing House, 1992. 169 p.

13. Yang W., Kuang J., Xu C. Formation conditions and prediction of large oilfields in Junggar Basin // Petroleum Geology of Xinjiang. 1995. Vol. 16. Iss. 3. P. 2101–2111.

14. Sun Z. Mesozoic-Cenozoic foreland basins in central and Western China and their hydrocarbon potential // Gas Geology. 1998. Vol. 4. Iss. 3. P. 16–301.

15. Zhang Z., Liou J., Coleman R.G. An outline of the plate tectonics of China // Geological Society of America Bulletin. 1984. Vol. 95. Iss. 3. P. 295–312. https://doi.org/10.1130/0016-7606(1984)95<295:AOOTPT>2.0.CO;2

16. Hsü K.J. Relict back-arc basins: principles of recognition and possible new examples from China // New perspectives in basin analysis / eds. K.L. Kleinspehn, C. Paola. New York: Springer, 1988. P. 245–263.

17. Argand E. La tectonique de l'Asie // Proc. 13th Int. Geol. Congr. 1924. Vol. 1. Iss. 5. P. 170–372.

18. Mooney W.D., Prodehl C., Pavlenkova N.I. Seismic velocity structure of the continental lithosphere from controlled source data (Chapter 54) // International handbook of earthquake & engineering seismology / eds. W.H.K. Lee, H. Kanamori, P.C. Jennings, C. Kisslinger. Part A. International Geophysics Series. Vol. 81A. Amsterdam – Boston – London – New York: Academic Press, 2002. P. 887–910.

19. Zhao J., Mooney W.D., Zhang X., Li Z., Jin Z., Okaya N. Crustal structure across the Altyn Tagh Range at the northern margin of the Tibetan plateau and tectonic implications // Earth and Planetary Science Letters. 2006. Vol. 241. Iss. 3-4. P. 804–814. https://doi.org/10.1016/j.epsl.2005.11.003

20. Zhao J., Jin Z., Mooney W.D., Okaya N., Wang S., Gao X., et al. Crustal structure of the central Qaidam basin imaged by seismic wide-angle reflection/refraction profiling // Tectonophysics. 2013. Vol. 584. P. 174–190. https://doi.org/10.1016/j.tecto.2012.09.005

21. Zhao J., Liu G., Lu Z., Zhang X., Zhao G. Lithospheric structure and dynamic processes of the Tianshan orogenic belt and the Junggar basin // Tectonophysics. 2003. Vol. 376. Iss. 3-4. P. 199–239. https://doi.org/10.1016/j.tecto.2003.07.001

22. Červený V., Molotkov I.A., Pšenčík I. Ray method in seismology. Prague: University Karllova, 1977. 214 p.

23. Feng R., Yan H., Zhang R. The method of quick inversion for 3D potential field and program designing // Journal of Geology. 1986. Vol. 4. P. 390–402.

24. Zhao J. Geodynamic conditions for northern margin of Tibetan Plateau. Beijing: Science Press, 2012.

25. Liu Y., Wu X. Wave velocity in rocks under high temperature and pressure and composition of the deep crust // Chinese Journal of Geophysics. 1997. Vol. 40. Iss. 3. P. 211–220.

26. Tilton G.R., Kwon S.T., Coleman R.G., et al. Isotoic studies from the west Junggar Mts, NW China // Geological Society of America, Abstracts with Programs. 1986. Vol. 18.

27. Xiao X., Tang Y., Li J., Jhu B. On the tectonic evolution of the northern Xinjiang, Northwest China // Xianjiang Geological Science. 1990. Vol. 1. P. 47–68.

28. Hopson C., Wen J., Tilton G., Tang Y., Zhu B., Zhao M. Paleozoic plutonism in east Junggar, Bogdashan, and eastern Tianshan, NW China // EOS, Transactions, American Geophysical Union. 1989. Vol. 70. P. 1403–1404.

29. Zhao J., Li Z., Cheng H., Yao C., Li Y. Structure of lithospheric density and geomagnetism beneath the Tianshan orogenic belt and their geodynamic implacations // Chinese Journal of Geophysics. 2004. Vol. 47. Iss. 6. P. 1061–1067.

30. Mooney W.D., Vidale J.E. Thermal and chemical variations in subcrustal cratonic lithosphere: evidence from crustal isostasy // Lithos. 2003. Vol. 71. Iss. 2-4. P. 185–193. https://doi.org/10.1016/j.lithos.2003.07.004

31. Wang F., Yang M., Zheng J. Geochemical evidence of the basement assembled by island arc volcanic terranes in Junggar basin // Acta Petrologica et Mineralogica. 2002. Vol. 21. Iss. 1. P. 1–10.

Information about the authors / Сведения об авторах

Junmeng Zhao,
Center for Excellence in Tibetan Plateau Earth Sciences, Chinese Academy of Sciences,
Beijing 100101, China,
Key Laboratory of Continental Collision and Plateau Uplift,
Institute of Tibetan Plateau Research, Chinese Academy of Sciences,
Beijing 100101, China,
University of Chinese Academy of Sciences,
Beijing 100049, China,
✉ e-mail: zhaojm@itpcas.ac.cn
Чжао Цзюньмэн,
Центр передового опыта наук о Земле Тибетского плато, Китайская академия наук,
100101, г. Пекин, Китай,
Главная лаборатория коллизии континентов и подъема плато,
Институт изучения Тибетского плато, Китайская академия наук,
100101, г. Пекин, Китай,
Университет Китайской академии наук,
100049, г. Пекин, Китай,
✉ e-mail: zhaojm@itpcas.ac.cn

Wenjiao Xiao,
University of Chinese Academy of Sciences,
Beijing 100049, China,
Institute of Geology and Geophysics, Chinese Academy of Sciences,
Beijing 100029, China
Сяо Вэньцзяо,
Университет Китайской академии наук,
100049, г. Пекин, Китай,
Институт геологии и геофизики, Китайская академия наук,
100029, г. Пекин, Китай

Xinfa Chen,
Xinjiang Oilfield Company,
Karamay 834000, China
Чэнь Синьфа,
Синьцзянская нефтяная компания,
834000, г. Карамай, Китай

Xiaojun Wang,
Xinjiang Oilfield Company,
Karamay 834000, China
Ван Сяоцзюнь,
Синьцзянская нефтяная компания,
834000, г. Карамай, Китай

Yong Song,
Xinjiang Oilfield Company,
Karamay 834000, China
Сун Юн,
Синьцзянская нефтяная компания,
834000, г. Карамай, Китай

Baoli Bian,
Xinjiang Oilfield Company,
Karamay 834000, China
Бянь Баоли,
Синьцзянская нефтяная компания,
834000, г. Карамай, Китай

Xiankang Zhang,
Center for Geophysical Exploration, China Earthquake Administration,
Zhengzhou 450000, China
Чжан Сянькан,
Центр геофизических исследований Сейсмологического управления Китая,
450000, г. Чжэнчжоу, Китай

Irina P. Strelchenko,
Key Laboratory of Continental Collision and Plateau Uplift,
Institute of Tibetan Plateau Research, Chinese Academy of Sciences,
Beijing 100101, China,
University of Chinese Academy of Sciences,
Beijing 100049, China,
Irkutsk National Research Technical University,
83 Lermontov St., Irkutsk 664074, Russia
Стрельченко Ирина Петровна,
Главная лаборатория коллизии континентов и подъема плато,
Институт изучения Тибетского плато, Китайская академия наук,
100101, г. Пекин, Китай,
Университет Китайской академии наук,
100049, г. Пекин, Китай,
Иркутский национальный исследовательсий технический университет,
664074, г. Иркутск, ул. Лермонтова 83, Россия

Qiang Xu,
Center for Excellence in Tibetan Plateau Earth Sciences, Chinese Academy of Sciences,
Beijing 100101, China,
Key Laboratory of Continental Collision and Plateau Uplift,
Institute of Tibetan Plateau Research, Chinese Academy of Sciences,
Beijing 100101, China
Сюй Цян,
Центр передового опыта наук о Земле Тибетского плато, Китайская академия наук,
100101, г. Пекин, Китай,
Главная лаборатория коллизии континентов и подъема плато,
Институт изучения Тибетского плато, Китайская академия наук,
100101, г. Пекин, Китай

Heng Zhang,
Center for Excellence in Tibetan Plateau Earth Sciences, Chinese Academy of Sciences,
Beijing 100101, China,
Key Laboratory of Continental Collision and Plateau Uplift,
Institute of Tibetan Plateau Research, Chinese Academy of Sciences,
Beijing 100101, China
Чжан Хэн,
Центр передового опыта наук о Земле Тибетского плато, Китайская академия наук,
100101, г. Пекин, Китай,
Главная лаборатория коллизии континентов и подъема плато,
Институт изучения Тибетского плато, Китайская академия наук,
100101, г. Пекин, Китай

Yingcai Zheng,
Massachusetts Institute of Technology,
Cambridge 02139-4307, United States of America
Чжэн Инцай,
Массачусетский технологический институт,
02139-4307, г. Кембридж, Соединенные Штаты Америки

Hongbing Liu,
Center for Excellence in Tibetan Plateau Earth Sciences, Chinese Academy of Sciences,
Beijing 100101, China,
Key Laboratory of Continental Collision and Plateau Uplift,
Institute of Tibetan Plateau Research, Chinese Academy of Sciences,
Beijing 100101, China
Лю Хунбин,
Центр передового опыта наук о Земле Тибетского плато, Китайская академия наук,
100101, г. Пекин, Китай,
Главная лаборатория коллизии континентов и подъема плато,
Институт изучения Тибетского плато, Китайская академия наук,
100101, г. Пекин, Китай

Bhupati Neupane,
Key Laboratory of Continental Collision and Plateau Uplift,
Institute of Tibetan Plateau Research, Chinese Academy of Sciences,
Beijing 100101, China,
University of Chinese Academy of Sciences,
Beijing 100049, China
Неупане Бхупати,
Главная лаборатория коллизии континентов и подъема плато,
Институт изучения Тибетского плато, Китайская академия наук,
100101, г. Пекин, Китай,
Университет Китайской академии наук,
100049, г. Пекин, Китай

Zongjin Ma,
Institute of Geology, China Earthquake Administration,
Beijing 100029, China
Ма Чжунцзинь,
Институт геологии Сейсмологического управления Китая,
100029, г. Пекин, Китай

Contribution of the authors / Заявленный вклад авторов

The authors contributed equally to this article.
Все авторы сделали эквивалентный вклад в подготовку публикации.

Conflict of interests / Конфликт интересов

The authors declare no conflict of interests.
Авторы заявляют об отсутствии конфликта интересов.

The final manuscript has been read and approved by all the co-authors.
Все авторы прочитали и одобрили окончательный вариант рукописи.

Information about the article / Информация о статье

The article was submitted December 22, 2020; approved after reviewing January 1, 2021; accepted for publication February 26, 2021.

Статья поступила в редакцию 22.12.2020; одобрена после рецензирования 20.01.2021; принята к публикации 26.02.2021.